Using NSBH tidal deformation for GW cosmography with 3G detectors

Shreya Anand *

September 22, 2017

*under the guidance of Dr. Alex Urban

1 Introduction and Motivation

1.1 Abstract

The past detections of Advanced LIGO have shown that current generation detectors have the capability to detect binary black holes at redshifts up to 0.2 [1]. Next generation detectors, however, with a factor of 10 increase in sensitivity compared to Advanced LIGO, are predicted to detect even binary neutron star (BNS) and neutron star-black hole (NSBH) sources to higher redshifts. We analyze a method of performing cosmography with third generation (3G) detectors using gravitational waves from NSBH inspirals alone. Cosmography requires independent measures of the distance to a source and and its redshift. Because gravitational wave sources are standard sirens, one can relate the source distance to its redshift by breaking the apparent mass-redshift degeneracy in the signal waveform. We consider a method of gravitational wave cosmography using tidal deformation signatures; assuming that the NS equation-of-state is known in the 3G era, we determine how well these signatures can be resolved by 3G LIGO-like detectors. Using waveform approximants that are valid in both inspiral and postmerger regimes to simulate NSBH waveforms with matter effects, we whiten the advanced LIGO data stream, inject the NSBH signals into the data stream, and attempt to recover tidal deformability signatures for both types of systems. Then, we recolor the current generation data stream using the modeled noise spectra for the next generation detectors Einstein Telescope and Cosmic Explorer. We determine how well tidal signatures can be recovered for systems of different mass, spin and tidal parameters, and use this to determine the targeted frequency bands for which current and next generation detectors should improve calibration uncertainty, as well as sensitivity. We aim to provide useful information for setting the calibration requirements for future 3G detector to enable cosmography with gravitational waves alone.

1.2 Overview of Cosmography Methods

Cosmography is the science of mapping or charting the universe at large. In the context of modern astrophysics, cosmography entails making precision measurements of cosmological parameters, which can be best understood as a relationship between the luminosity distance to the source and its cosmological redshift:

$$D_L = \frac{c(1+z)}{H_0} \int_0^z \frac{dz'}{[\Omega_M (1+z')^3 + \Omega_\Lambda (1+z')^{3(1+\omega)}]^{1/2}} \tag{1}$$

where H_0 is the Hubble constant, z is the redshift, c is the speed of light, Ω_M and Ω_Λ are the dimensionless matter density and dark energy density parameters of the universe, and ω determines the equation of state of dark matter[4]. In the local universe, one can make measurements of the Hubble constant; the other cosmological parameters can only be constrained using sources from the high-redshift universe.

In order to constrain the values of these cosmological parameters, one requires an independent measure of both the redshift and the luminosity distance to the source. One of the most popular methods involves using white dwarf supernovae as standard candles. The most viable model for creating such explosions, known as the doubly degenerate model, is hypothesized to occur when a merger of the white dwarfs exceeds the Chandrasekhar limit. The model predicts a precise intrinsic luminosity such that measuring the observed flux constrains the distance to the supernova. By measuring the observed flux of the Type Ia supernova, one can determine the distance to the source. More recent evidence suggests that that before using Type Ia supernovae as standard candles, one must correct for their lightcurves (which follow an established trend) and then calibrate their peak brightness using cepheid variable stars, one rung down from Type Ia supernovae in the cosmic distance ladder. The calibrated peak brightness would provide the distance to the source. Independently, one can determine the redshift of the source, using standard methods to analyze the SNe spectrum [2]. However, currently, such measurements face large systematic errors due to the fact that their progenitor composition is still largely a mystery [3]. Using cosmographical measurements from Type Ia supernovae, astronomers determine H_0 to be 73 km s^{-1} Mpc^{-1} with a one percent errorbar [2].

However, recent measurements made by the Planck satellite determine the Hubble parameter to be closer to 67 km s^{-1} Mpc^{-1} [4] within two percent error. This secondary method employs the CMB power spectrum to determine the characteristic size scale of structure formation (baryon acoustic oscillation radius) and relate it to the redshift at which the CMB began radiating ($z \approx 1089$). This large discrepancy regarding the acceleration rate of expansion of the local universe could be reconciled using gravitational wave cosmography.

There are a few different proposed methods for performing cosmography using gravitational wave signals from both binary neutron star mergers and neutron star-black hole mergers. One such method involves a coincident short GRB observation with a BNS or NSBH inspiral signal detection. Using the spectra of the optical counterpart of such an event, one can either determine redshift using spectral analysis, or localize the source to its host galaxy and thereby infer the source redshift from the galaxy's redshift. From the GW signal-to-noise ratio, one can find the distance independently, using the equation relating S/N to distance, D:

$$\rho \propto \frac{1}{D} \int_{f_2}^{f_1} \frac{f^{-7/3}}{S(f)} df \tag{2}$$

where ρ is the signal to noise ratio, S(f) is the noise as a function of frequency, $f^{-7/3}$ is the approximate scaling law of a BNS merger signal, and the expression is integrated from the lower bound of the frequency range the detector is sensitive to (20-30 Hz for Advanced LIGO) to the upper bound of the frequency at which the merger is expected to occur (this frequency is referred to as f_{ISCO}, which is a function of the masses of the sources in the system) [6]. Because gravitational wave signals are well-modeled by numerical relativity, they are considered to be standard sirens, since we can obtain the distance to the source using its amplitude or S/N.

Since the measures of redshift and distance described above are calibration-independent, compact binary coalesences have the potential of being used in a way analogous to Type Ia supernovae to measure distance scales (and the expansion rate) of the universe. An alternate method has been outlined in [11] to measure the redshift of the BNS or NSBH merger by locating the signature of tidal disruption in the gravitational wave signal itself. Such a measurement would require a high enough signal-to-noise ratio to be able to easily distinguish from the noise. Currently, by assuming a cosmological model as well as values for the cosmological parameters in equation 1, one can infer the source-frame masses. However, if with next generation detectors we are able to tightly constrain the neutron equation of state, then, using the frequency at which tidal deformation occurs, one can break the degeneracy between mass and redshift, and thereby find both redshift and distance from the gravitational wave signal alone. A secondary, alternate method has also been outlined in [11] in which a typical BNS merger results in a hypermassive neutron star (HMNS) in the postmerger phase, that delays formation into a black hole, and has a unique signature in the gravitational wave signal that can be used to break the mass-redshift degeneracy. However, such studies are only possible with next generation detectors. The signal-to-noise ratios, as well as the sensitivities to distant sources are too low using second generation detectors; thus, this study, which will focus on the tidal deformation method of cosmography with gravitational waves, involves networks of next generation detectors.

1.3 Next Generation Detectors

Below, we provide a brief summary of each of the next generation detectors:

• A+: This incremental upgrade to the advanced LIGO detectors includes better coatings, quantum light squeezing, and heavier test masses [7] than the current detectors. According to a presentation from the 2016 DAWN workshop, because aLIGO is limited by quantum noise at both high and low frequencies, this detector will employ frequency dependent light injection squeezing for the purpose of quantum noise reduction [9]. In the middle band, since aLIGO is dominated by brownian thermal noise in the mirror coatings, the proposed design for A+ has full aperture coatings that will improve the mid-band sensitivity. A+ is predicted to have a factor of 1.7 increase in range and factor of 5 increase in event rate over aLIGO without a significant monetary investment, and as a low-risk operation. Optimistically, A+ should come online within the next 6.5 years [9].

• Einstein Telescope (ET-D): Located in Europe, ET-D is a proposal for an underground detector, with 10 km arms connecting three detectors in a triangle configuration. A 2011 design study on Einstein Telescope predicts that each detector will comprise of two interferometers, one for detecting high frequencies and the other for low frequency signal detection, in a xylophone configuration. The high frequency (HF) interferometer will employ the techniques of using high laser light power in the Fabry-Perót cavities, as well

as frequency dependent squeezed light to reduce quantum noise. On the other hand, the low frequency (LF) interferometer will suppress the thermal, seismic, gravity gradient, and radiation pressure noise sources by functioning at a cryogenic temperature. Furthermore, since it will be located underground, ET-D should have increased sensitivity in the low (2 - 50 Hz) band [8].

• Cosmic Explorer (CE): The most ambitious project of the three, CE, will be an L-shaped detector with 40 km arms designed to minimize noise sources besides gravitational waves [7]. This detector, however, is in its very early stages of design and development, and will likely be the last amongst the three next generation detectors discussed, to come online. According to a study of next generation detectors by the LIGO Scientific collaboration as well as our analysis presented in a later section of the thesis, Cosmic Explorer should have the capability to detect high redshift sources (z $>$ 4) at signal-to-noise ratios (S/N) of 8. This detector's ability to minimize the various noise sources identified in the LIGO study will determine its sensitivity [10]. The calibration sensitivity then informs how well both intrinsic and extrinsic parameters can be observed.

1.4 Conditions for Tidal Deformation

Amongst the types of systems we anticipate to observe using ground-based gravitational observatories, only systems with neutron stars are capable of tidally deforming during their inspiral and merger phases. Just as the Earth bulges due to the gravitational influence of the Moon on it at certain points during the Moon's orbit around the Earth, either one or both the masses in the compact binary stretch and squeeze due to the influence of the other body. Black holes lack surfaces, and therefore for the types of systems we examine, only neutron stars experience tidal deformation. While all BNS systems undergo tidal deformation and eventuallly disruption at the time of merger, only under certain conditions, the neutron stars in NSBH systems are tidally deformed; the conditions rely on the mass ratio between the black hole and the neutron star, as well as the black hole spin. [1] If the neutron star is much less massive than the black hole, it is likely to simply be consumed by the black hole following its inward inspiral, producing no EM counterpart or tidal disruption signature in the gravitational waveform. For a certain range of mass ratios between black holes and neutron stars, the neutron star first tidally deforms as the neutron star and black hole inspiral towards one another; then upon merger the black hole disrupts the neutron star surface, and the NS matter forms an accretion disk around the black hole. However, according to [12], neutron stars in neutron star-black hole systems with mass ratios between 3 and 5 are most likely to tidally deform, for lower spin black hole companions. As shown in the figure below for systems of mass ratio greater than 5, more extremally spinning black holes are needed to tidally deform neutron stars. The red region shows the regions of mass ratio-spin parameter space for which we do not expect tidal deformation; the blue and green regions correspond to tidally deforming neutron stars with a remnant disk mass of $0 \geq m_{disk} \geq 0.2m_{NS}$ and a massive disk of $m_{NS} \geq 0.2M_{sun}$ respectively.

The primary systematic bias associated with determining tidal signatures of matter in NSBH gravitational waveforms is that the equation of state of neutron star is unknown as of yet. Therefore, we can characterize the strength of the deformation using a tidal parameter, Λ, given by

$$\Lambda = \frac{2k_2}{3}\left(\frac{R}{M}\right)^5 \tag{3}$$

where k_2 is the neutron star tidal Love number, R is the radius of the star, and M is the neutron star mass, and using a given equation of state model relating the neutron star mass to its radius, find Λ as a function of the NS mass alone. Clearly, given the factor of $(\frac{R}{M})^5$ in the calculation of Λ, one can see that Λ is a strong function of the equation-of-state of the star. In our study we consider APR and 2H as two possible equations of state, where APR, with a lower deformability parameter for a NS with a given mass is a moderate equation-of-state, while the 2H model is a more extreme EOS model with higher Λ parameters on average. We analyze the signal-to-noise ratio of deformability signatures and determine its scaling with

[1] Conceivably, neutron star spins also contribute to conditions for tidal deformation. However, neutron star dimensionless spins can only extend up to 5 percent of the maximum possible black hole spin. Since they are comprised of matter, neutron stars could break apart if their rotation exceeds the spin limit, while black holes, intrinsically containing no matter, are only restricted by the conditions imposed by general relativity.

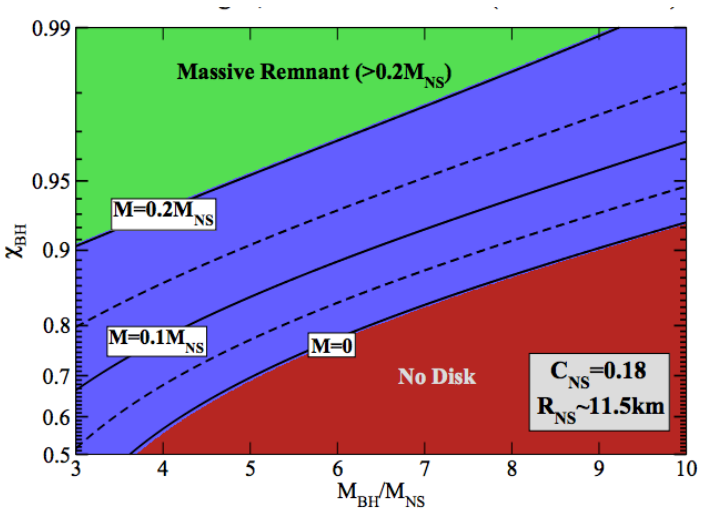

Figure 1: Regions in mass-spin space where tidal deformation is more likely to be observed

mass ratio of the two sources. Another parameter, λ, used in certain conventions, is defined as $\lambda = \frac{2kR^5}{3G}$, where R is a function of M determined by the neutron star EOS. For example, using the 2H EOS, λ ranges from about 10,000 at a neutron star mass of 1 M_{sun} to around 200 at a neutron star mass of 2 M_{sun}.

We use the state-of-the-art waveform model for NSBH systems, the Lackey Tidal 2013 SEOBNRv2 ROM approximant [13] to simulate our NSBH systems. Because the TaylorF2 approximant uses the stationary phase approximation, it is valid in the inspiral-only regime. Other waveforms from the IMRPhenom family do not account for tidal effects in the waveforms. Since the matter signatures we search for will either be post-merger oscillations or be present in the early inspiral, we require a waveform approximant computed using numerical relativity. The Lackey tidal waveform is a reduced order model, using the single effective one body method to calculate the NSBH inspiral and ringdown, calibrated to numerical relativity [13]. We choose the Lackey waveform to obtain the greatest possible accuracy while minimizing computational cost. However, since the Lackey tidal waveforms have specifications for the source parameters, we can only consider systems with neutron star masses of 1.4 M_{sun} or greater. The specifications for Lackey are as follows: $\lambda_{NS} \leq 4382$, $M_{TOT} \geq 2M_{sun}$ at 10 Hz, $-0.5 \leq \chi_{BH} \leq 0.5$, and $2/9 \leq \eta \leq 5/6$, where η is the symmetric mass ratio. Using the limits for η we determine that the mass ratio of the black hole to the neutron star must range from 3-5 [13]. Using the parameter specifications for Lackey, combined with our assumption that $1M_{sun} \leq m_{NS} \leq 2M_{sun}$ and $5M_{sun} \leq m_{BH} \leq 15M_{sun}$ we choose the parameters of our source systems (see section 2.1).

1.5 Breaking the Mass-Redshift Degeneracy

Gravitational wave signals provide an accurate measure of the chirp mass of the gravitational wave source, rather than the individual source component masses. The chirp mass is given by:

$$M_{chirp} = \frac{(m_1 m_2)^{3/5}}{(m_1 + m_2)^{1/5}} \tag{4}$$

which can also be re-expressed in terms of gravitational wave frequency. However, the measurement of the chirp mass from the signal is redshifted; for previous detections, we have assumed a given cosmological model (usually Friedmann-Robertson-Walker) and used the latest measurements of H_0, Ω_Λ, Ω_M, and ω, to determine the redshift of the binary black hole source from the distance formula given by equation one. However, the objective of cosmography is to determine how the distance relates to the measured redshift, so in order to do cosmography using gravitational wave measurements alone, we require a way of breaking the mass-redshift degeneracy. A visible signature of the black hole disrupting a neutron star in a NSBH coalescence waveform would provide us precisely with that. By plotting the fourier transform of the NSBH gravitational waveform, one can determine the frequency at which tidal disruption occurs. We can re-express the frequency of gravitational waves in terms of the masses in the binary, using the fact that the

gravitational wave frequency, $f_{GW} = 2f_{orb}$, the orbital frequency. Although in reality, the orbital frequency is derived from full general relativity, we can obtain a zeroth order approximation of it using Kepler's 3rd law and the relationship between the radius of innermost stable circular orbit (ISCO) of a black hole and its spin parameters.

ISCO is a purely general relativistic phenomenon that occurs for binary systems in strong gravitational regimes. In systems with a black hole, ISCO is the radius of a particle's orbit around the black hole at beyond which it can no longer maintain a stable circular orbit. At ISCO, the energy radiated away as gravitational waves equals the angular momentum loss, and beyond this radius, angular momentum dominates, resulting in the particle's inevitable inspiral into the black hole.

For NSBH systems, we assume that the frequency at which the neutron star is tidally disrupted is equivalent to the ISCO frequency of a black hole of mass equivalent to the total mass of the system. For such a black hole, from the Kerr metric, we obtain:

$$a_{ISCO} = \frac{6GM_{BH}}{c^2}(3 + Z_2 \mp \sqrt{(3 - Z_2)(3 + Z_1 + 2Z_2)}) \tag{5}$$

Here, $Z_1 = 1 + (1-\chi^2)^{1/3}[(1+\chi)^{1/3} + (1-\chi)^{1/3}]$, and $Z_2 = (3\chi^2 + Z_1^2)^{1/2}$, and χ is the dimensionless spin parameter J/M^2, where J is the angular momentum of the black hole, and M_{BH} is the black hole's mass. Then, $f_{orb} = 2\pi$ / T, where T is defined by Kepler's 3rd law as:

$$\frac{R^3}{T^2} = \frac{G(m_1 + m_2)}{4\pi^2} \tag{6}$$

and, replacing T with $1/f_{orb}^2$, we can write, in terms of the system parameters:

$$f_{orb}^2 = \frac{G(m_1 + m_2)}{4\pi a_{ISCO}^3} \tag{7}$$

But a_{ISCO} is a function of the spin parameters, so we can express the gravitational wave frequency, $f_{GW}^2 = 4 * f_{orb}^2$,in terms of the equivalent black hole mass and spin parameters, and some constants:

$$f_{GW} \approx \frac{c^3}{GM_{BH}}(3 + Z_2 \mp \sqrt{(3 - Z_2)(3 + Z_1 + 2Z_2)})^{-3/2} \tag{8}$$

Since we are looking at tidal disruption, we recognize that the gravitational wave frequency is the same as the ISCO frequency, where tidal disruption occurs. Writing this more compactly in terms of $S(\chi)$, the dimensionless portion of the a_{ISCO} expression containing all of the spin parameters, we find:

$$f_{TD} \approx \frac{c^3}{GM_{BH}} S(\chi)^{-3/2} \tag{9}$$

Of course, in order to find the true tidal disruption frequency of the system, or the ISCO frequency of the equivalent black hole, we need to perform the calculation in general relativity. Nevertheless, this method can be employed to find the zeroth order approximation for the way the ISCO frequency scales as a function of the total mass of the system. Identifying the frequency at which tidal disruption occurs will allow us to relate the mass that we measure, $M_{chirp}(1+z)$ to the tidal disruption frequency we derived, and calculate the mass and redshift using a system of equations. Similarly, if we identify the frequencies of observed tidal deformation signatures, we can break the mass-redshift degeneracy in gravitational waveforms. Thereby, the main limiting factor to how well we can measure the redshift using this method is our ability to determine the tidal disruption or deformation frequencies from the signal's fourier transform.

2 Methodology

2.1 Waveform Visualization

For each source system, we plot the frequency-domain gravitational wave signal (magnitude and phase components) for three different cases: 1) no tidal deformation, 2) neutron star with APR equation of state,

and 3) neutron star with 2H equation of state. For systems in which there are no matter effects involved, one can distinguish by eye the difference between a system with a black hold of spin zero and a black hole with spin parameter 0.5. Our plots depict systems with spin in color, and systems with no spin in black dashed lines. In magnitude, the difference between systems with and without spin is only visible in the high frequency regime; however in phase, one can distinguish between systems with and without spin starting frequencies of 400-500 Hz, close to our rough estimates for f_{ISCO}. Though we have calculated estimates of the ISCO frequencies of the systems, using the method outlined in the previous section, we allow the waveforms to continue until they automatically cutoff using the Lackey tidal approximant. We observe that a system with a mass ratio of 5 cuts off at a higher frequency in magnitude as compared to the system with a mass ratio of 3; the phase evolution for the three sets of systems show distinct morphologies.

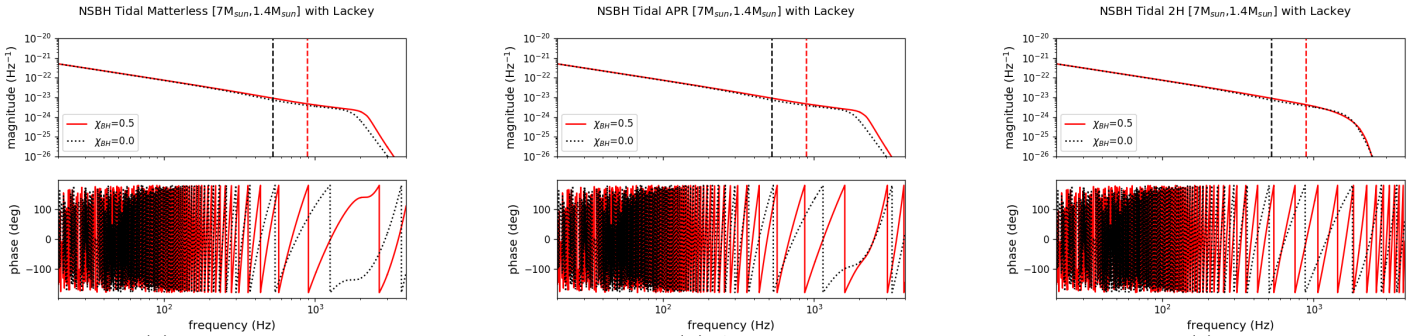

(a) no matter effects (b) APR EOS (c) 2H EOS

Figure 2: Plotting simulated waveforms for $1.4M_{sun}$ $7M_{sun}$ NSBH for different EOS models

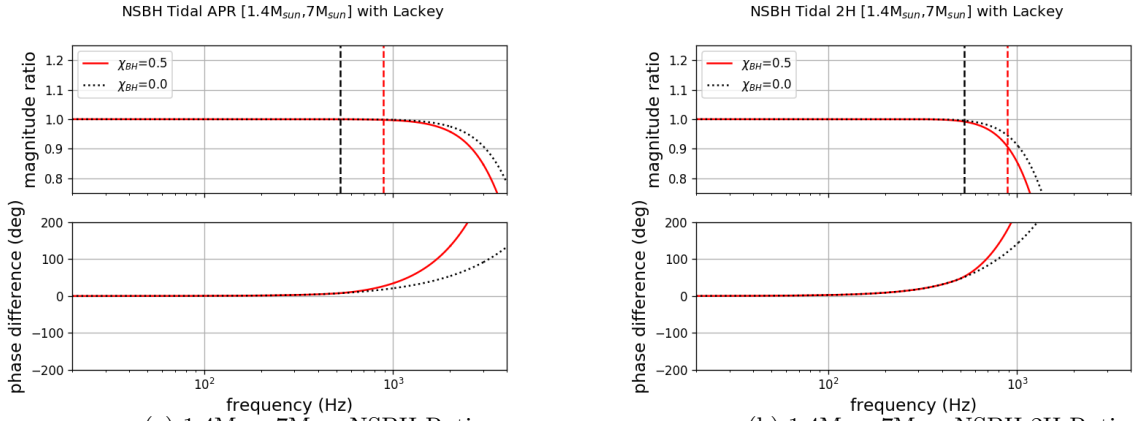

(a) $1.4M_{sun}$ $7M_{sun}$ NSBH Ratio (b) $1.4M_{sun}$ $7M_{sun}$ NSBH 2H Ratio

Figure 3: Ratio of simulated waveforms for $1.4M_{sun}$ $7M_{sun}$ NSBH systems

Next, we use the APR and 2H equation of state models to observe matter effects in the gravitational waveform. On average, the deviation between matterless waveforms and waveforms with tidal effects, holding all other parameters fixed, is far more clearly visible when assuming the 2H equation of state model, and in general, the difference in phase between waveforms with and without matter effects is more obvious than the difference in magnitude. As outlined in the previous section, breaking the mass-redshift degeneracy involves identifying the frequency at which matter signatures are clearly present in the gravitational waveform. We quantify these matter signatures by dividing the simulated waveforms with matter effects for a given set of mass and and spin parameters by the corresponding matterless waveform. In magnitude, this operation constitutes a ratio, while in phase, we subtract the waveforms; the first place where the ratio (or difference) deviates from one (or zero) we take to be the approximate frequency at which the matter signature is present.

Since we are examining waveforms for sources that are a distance of 10 Mpc away (very low redshift), the frequency of the deformability signature in magnitude appears above 1 kHz for all of the systems we examined. The high levels of noise on the high frequency end hinders identification of these postmerger tidal

m_{BH} (M_{sun})	m_{NS} (M_{sun})	χ_{BH}	f_{mag} (Hz)	f_{phase} (Hz)	radius (km)	Λ
7.0	1.4	0.5	1323.0	417.2	11.53	269.751
7.0	1.4	0.0	1540.1	417.2	11.53	269.751
6.4	1.6	0.0	1802.9	525.9	11.45	110.234
6.4	1.6	0.0	2113.7	527.2	11.45	110.234
5.4	1.8	0.5	2463.9	651.2	11.31	44.74
5.4	1.8	0.0	2901.6	661.2	11.31	44.74

Table 1: Tidal and source parameters for systems with APR EOS

m_{BH} (M_{sun})	m_{NS} (M_{sun})	χ_{BH}	f_{mag} (Hz)	f_{phase} (Hz)	Λ
7.0	1.4	0.5	544.70	143.4	1819.35
7.0	1.4	0.0	605.50	143.4	1819.35
6.4	1.6	0.5	653.40	170.4	841.404
6.4	1.6	0.0	733.60	170.4	841.404
5.4	1.8	0.5	783.70	194.7	405.821
5.4	1.8	0.0	884.30	194.7	405.821

Table 2: Tidal source parameters for systems with 2H EOS

effects in magnitude. In phase, however, differences between waveforms with and without matter show up between 100 and 700 Hz using both EOS models (depending on the mass ratio of the system). Therefore the difference between the phase component of waveforms with and without matter manifests itself as a lower frequency signature during the inspiral stage. Interestingly, for the 2H equation of state model, systems with identical mass parameters, with and without spin have the same tidal signature frequency, varying from roughly 150 - 200 Hz, from high to low mass ratio. Since spin is a higher order effect, at such low frequencies, we cannot distinguish between waveforms with and without spin. As our table suggests, though, the deformation signatures occur at higher frequencies for the APR equation of state, so using phase information alone, one can distinguish between systems with and without black hole spin for mass ratios of 3 and 4.

Spin plays an important role here, since as we witnessed earlier, waveforms with and without spin have different morphologies in magnitude and especially in phase. If we must rely on matter signatures in phase primarily because in magnitude the signatures occur at frequencies well above our sensitive regime, then being able to distinguish between systems with and without spin will eliminate a potential systematic bias in determining whether what we observe is actually a matter signature or not.

We record the frequencies at which matter signatures are present in magnitude and phase for the APR and 2H equation of state models, and report them in tables 1 and 2.

2.2 Constructing Simulated Data

In order to determine whether the tidal signatures of matter would be visible in our waveforms, we conduct an experiment in which we inject our simulated signals into the detector datastream and attempt to recover the tidal signatures that were present in the simulated signal. However, as we are interested in the observability of these signatures with next generation detectors, we simulate the datastream of the next generation detector ET. Recoloring the Advanced LIGO datastream with the noisecurve of ET provides a more realistic measure of how well we can recover tidal signatures of matter than simply comparing the signal amplitude across frequencies to the predicted amplitude spectral density of a third generation detector.

We begin by reading in raw h(t) strain data from the LIGO Livingston datastream using the GDS-CALIB-STRAIN channel. We divide out all effects of the Advanced LIGO noisecurve, or in other words whiten the data against its own ASD, computed using an FFT length of 4 seconds and overlap length of 2 seconds, and plot the whitened strain as a function of time. The main characteristic of whitened data is that

it contains only uncorrelated, or white noise. The aim of whitening the data is to remove any association of the strain data with the noisecurve of the Advanced LIGO detector. To check whether the whitening was successful, we plot the whitened ASD of our datachunk, and find that indeed, the ASD is centered around 1 (indicating no correlation present) with some sharp peaks corresponding to the white noise.

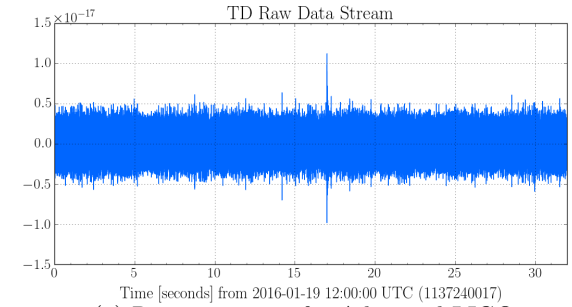

(a) Raw timeseries for Advanced LIGO

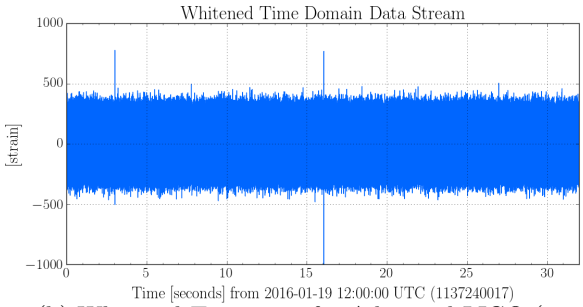

(b) Whitened Timeseries for Advanced LIGO (32 s)

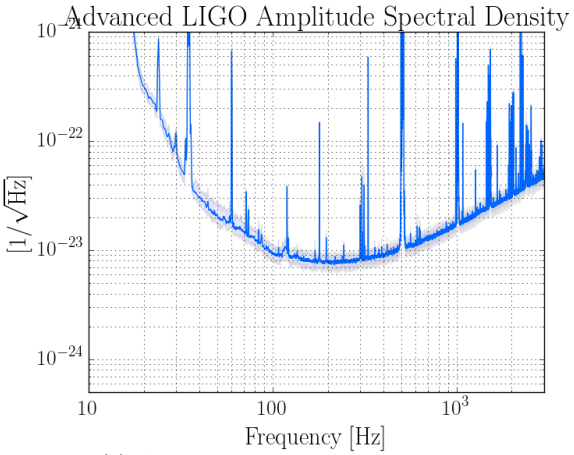

(c) ASD with 5th and 95th percentiles

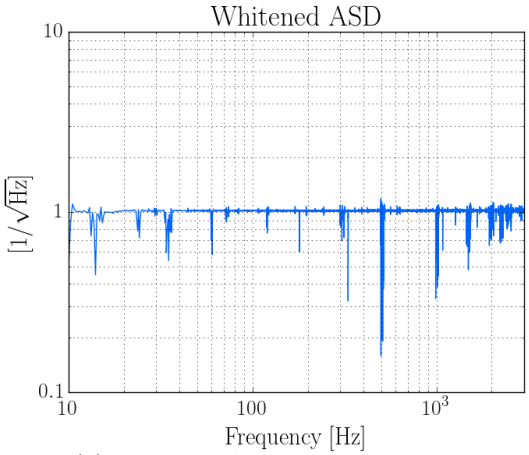

(d) Whitened ASD for Advanced LIGO

Figure 4: Figures illustrating the process of whitening the Advanced LIGO raw timeseries data

We can effectively multiply this random, uncorrelated noise with the ASD of a next generation detector (or, for that matter, divide it by the inverse of a given detector's ASD) and create a recolored datastream for that future detector. Recoloring reverses the whitening operation; if we were to recolor the whitened datachunk with the ASD of Advanced LIGO that we computed earlier, we would retrieve the original strain data that we had read in. Instead, we recolor the whitened datastream with the noisecurve of ET, and plot the recolored datastreams along with their corresponding ASDs. In our ASD plots, the red dotted curve shows the theoretical noisecurve for each of the detector. As the figures suggest, our recoloring of the original datastream with ET's noisecurve was successful; the resulting ASD has the same shape we expect, with additional noise contributions visible in our whitened ASD plot.

Now, equipped with the necessary components, the simulated signal and the simulated next generation detector datastreams, we can perform our signal injection.

3 Results

3.1 Signal Injection and Retrieval

As compared to the whitening and recoloring processes, injecting the astrophysical signal into the datastream of an advanced detector is far more straightforward. For the injection, we tapered the signals at both ends to zero, and then simply added them to the recolored datastreams. Figure 6 displays the theoretical signal as a function of time on the top axis, along with the injected signal on the bottom axis. The primary distingushing characteristic between the two is the noise contamination in the bottom plot due to the

addition of noise; the astrophysical signal, however, dominates for the case of ET over the noise floor.

When examining the signal in the frequency domain, one can clearly see that unlike the white noise which uniformly affects all frequencies the same way (as demonstrated by the flat whitened ASD of Advanced LIGO, the recolored datastream of Einstein telescope does experience more noise contamination at higher frequencies, especially for frequencies greater than 1 kHz. We observe the effects of noise dominating at higher frequencies in both the signal magnitude and phase in the frequency domain.

Upon examining the signal-to-noise ratio distribution as a function of frequency, we observe that the S/N is highest around 10 Hz for Einstein Telescope, and decreases slowly from about 10^5 down to 10^3, experiencing a steep decline past frequencies of about 2.5 kHz for both 2H and APR EOS models. While this implies that tidal signatures in the magnitude of frequency-domain waveforms will be quite difficult to identify due to the noise floor at those frequencies, the phase signatures during the inspiral should still be clearly visible. Although only a small fraction of the maximum signal to noise ratio is distributed between 100-700 Hz, where we expect to see phase signatures, figure 6b of the signal injection suggests that during the inspiral phase, the signal clearly dominates over ET's noisecurve, implying that matter signatures in phase, during the inspiral, are more promising for extracting signal redshift, as compared to postmerger signatures in magnitude.

Integrating the signal-to-noise ratio over the range of frequencies that ET is sensitive to results in a very high S/N for nearby NSBH sources; however, even so, our injection indicates that the noise levels of the detector datastream will make picking out the tidal signatures at high frequency in magnitude a challenging task. That being said, the NSBH systems we observe will be much farther than 10 Mpc in luminosity distance, and so the effects of redshift will become important in determining how well we can observe the frequency of tidal signatures.

3.2 S/N Scaling with Redshift

While the overall signal-to-noise ratio of BNS and NSBH systems may not be as informative as the signal-to-noise ratio scaling with frequency for identifying the tidal deformation signatures, knowing to what redshifts we can anticipate being able to detect BNS and NSBH systems with ET will help place constraints on our ability to do cosmography. Since the signal-to-noise ratio of a signal is inversely proportional to the distance to the source, we can determine how the signal-to-noise ratio scales with redshift by assuming a standard ΛCDM cosmology and using the relationship between the luminosity distance and redshift determined by measurements from Planck. We integrate the signal-to-noise ratio from 10 Hz up to the redshifted frequency at which the tidal waveforms cutoff, iterating over redshifts from 0 to 100, uniformly spaced in logspace.

From our plots, we can gather that with next generation detectors, there is a vast improvement in how far into the universe we can probe NSBH sources. Repeating this study for BNS systems, we found that the signal-to-noise ratio scaling with redshift was not a very strong function of mass, and predicted similar signal-to-noise ratios for BNS detections with next generation detectors (though we only consider relatively

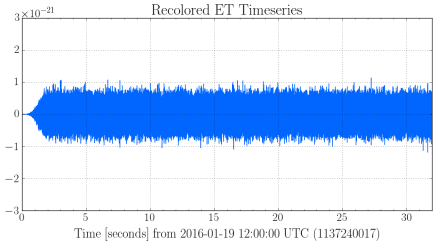

(a) Recolored timeseries for ET-D (32 s)

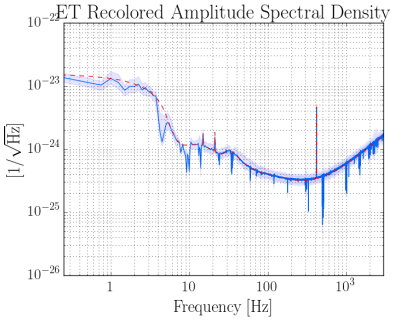

(b) Recolored ASD for ET-D

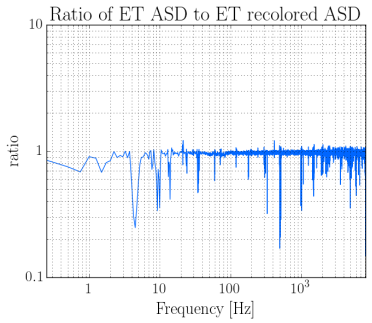

(c) Ratio between original and recolored ET ASD

Figure 5: Figures illustrating the process of recoloring the Advanced LIGO datastream with ET-D noise ASD

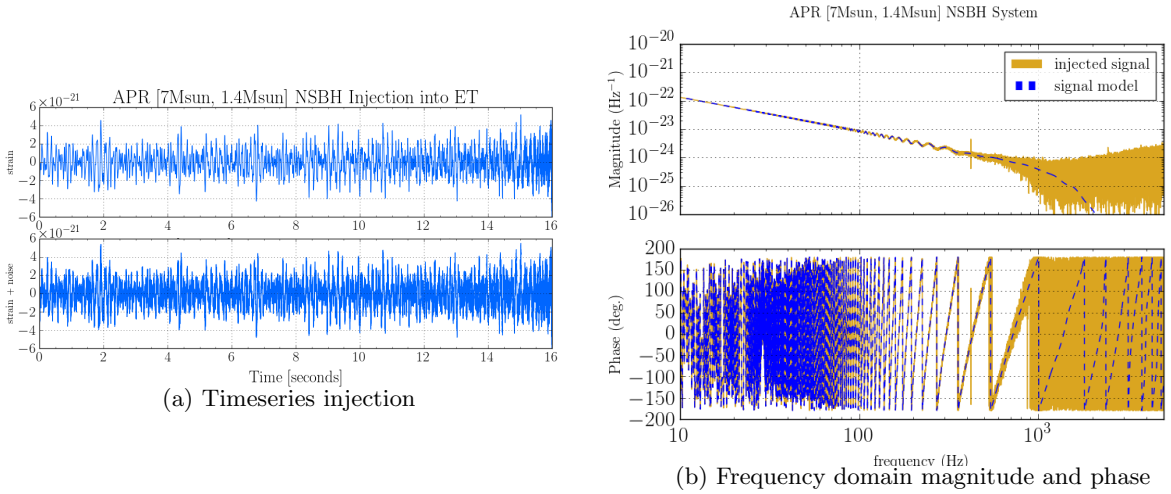

(a) Timeseries injection

(b) Frequency domain magnitude and phase

Figure 6: Signal injection in time and frequency domain with APR EOS

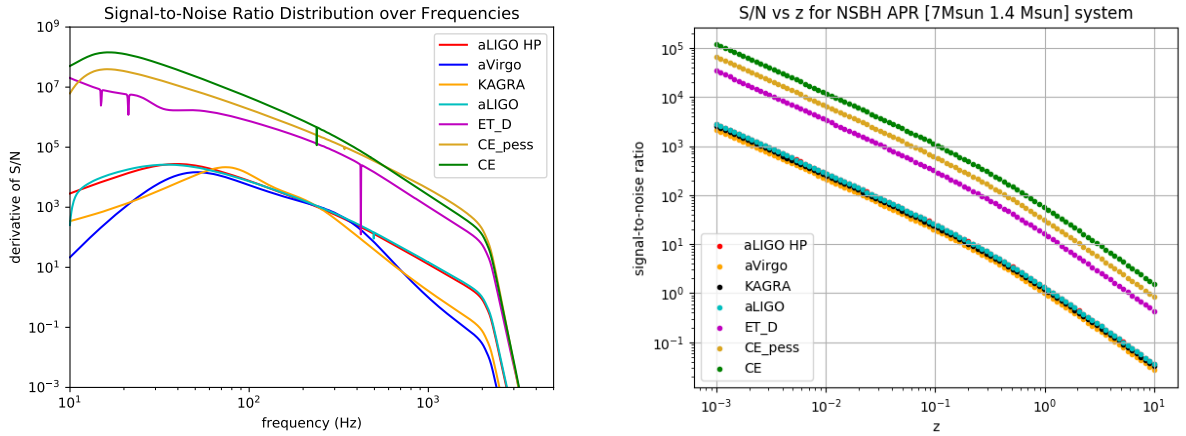

(a) S/N distribution over frequencies

(b) S/N as a function of redshift

Figure 7: Signal-to-noise ratio and its derivative for APR EOS with current and next generation detectors

low-mass black hole components, as only those systems satisfy a maximum mass ratio of 5). Specifically, we examine the threshold S/N ($\rho = 8$) for each detector and use this to determine to what redshift each detector can probe an NSBH (or a BNS) system at. Advanced LIGO at design sensitivity can probe systems out to z $\approx$ 0.3 with $\rho = 8$, while at a redshift of 1 aLIGO has $\rho \approx 1$, demonstrating that even for sources considered nearby on a cosmological distance scale, Advanced LIGO will not detect BNS and NSBH systems with a high enough overall signal-to-noise ratio to be able to confidently resolve tidal deformation signatures in the waveform. From this plot, we can predict that Einstein Telescope, on the other hand, will detect BNS and NSBH systems from redshift 1 with signal-to-noise ratios of about 11, and can detect BNS and NSBH systems until z $\approx$ 2 above the threshold S/N. If we achieve the most optimal noise floor for Cosmic Explorer, then the detector should theoretically have the capability to detect systems until redshifts of nearly 5 with S/N of 8. Thus ET, promising a factor of 10 in improvement in signal to noise ratio over Advanced LIGO, and CE, offering a factor of 4 improvement over ET, will not only be capable of constraining H_0, but could also help constrain other cosmological parameters, as they can both probe the high redshift universe.

The detectability of tidal signatures themselves, however, is another matter. As detailed by the previous section, the signal-to-noise ratio distribution over frequencies, rather than the overall signal-to-noise ratio, determines how well we can identify tidal signatures at the frequencies that we expect to observe tidal signatures. However, since redshift decreases the frequencies we observe as compared to the frequencies at which the gravitational waves were emitted, the tidal deformation frequency will also be redshifted down by a factor of (1+z). Thus, we plot the redshifted tidal deformation frequency in magnitude as a function

of redshift. Assuming that the APR equation of state is more realistic in comparison to the 2H equation of state, the tidal signatures we have identified in magnitude occur at higher frequencies for lower mass-ratio systems and systems with non-zero spin. For non-spinning nearby systems with mass ratios of 5, this deformation frequency occurs slightly above 1 kHz. However, if such a source is found past redshifts of around 0.5, the observed deformation frequency will begin to drop below 1 kHz and decline rapidly with increasing redshift. For an NSBH system found at a redshift of 1, the deformation signature would occur around 550Hz, comfortably in the sensitive band of ET. Therefore redshift appears to improve our ability to locate signatures of tidal deformation in NSBH waveforms, with the APR equation of state. The 2H equation of state experiences a similar scaling of deformation frequency with redshift, aside from the fact that the magnitude deformation frequencies for each of the systems (with corresponding mass ratio and spin) all occur below 1 kHz for very nearby sources. Since the phase deformation signatures are already visible, redshift will result in them appearing at even lower frequencies, transitioning from the sensitive portion of the detector band down to 10 Hz. Because Einstein Telescope has sensitivity to sources of only $z \approx 2$, redshift should not contribute significantly to detectability of tidal signatures in signal phase. Thus we are more likely to identify deformation signatures in frequency for NSBH systems, if indeed neutron stars have extreme equations of state more akin to 2H. Having examined the effect of a recolored datastream on signal detectability, we investigate the effect of calibration uncertainty on detectability of tidal signatures for the purpose of cosmography.

3.3 Calibration Uncertainty

Our ability to constrain H_0 from tidal deformation signatures is dependent on the uncertainties in signal phase and amplitude in the frequency-domain gravitational waveform. Both systematic and statistical uncertainties affect our ability to measure these matter signatures in the gravitational waveform. Here, we differentiate between uncertainties in amplitude and phase arising from purely statistical (Bayesian) uncertainties, statistical calibration uncertainty, and systematic calibration uncertainty. One can use a Fisher matrix analysis to determine the Cramer-Rao bound on the calibration uncertainties in source distance, signal phase and signal amplitude, thereby determining the effect of calibration uncertainty on determining the redshift of the source. However, we leave this as a subject of a future, more in-depth study. For now, using the overall calibration uncertainty budget for L1 [14] we can predict both the statistical and systematic calibration uncertainty levels at the frequencies we expect to see deformation signatues in magnitude and phase.

The overall calibration uncertainty budget, in the frequency domain, is a complex number with magnitude and phase components. This uncertainty arises from the fact that the LIGO interferometer does not directly measure astrophysical strain; rather the detector goes through a feedback control loop process to reconstruct the gravitational wave strain. In the control loop process, either noise, or a passing gravitational wave with its associated noise, enters the detector, causing a residual arm length change in the interferometer, inducing a laser light signal in the detector readout port. The sensing function converts these light pulses into a digital error signal. The error signal is converted to a control signal through the digital filter, and then fed to the actuation function, which translates this signal into residual arm length changes in the detector, reconstructing the gravitational wave signal. While the digital filter has no associated uncertainty, in reality both the actuation and sensing functions differ from their corresponding models due to uncertainties in the actuation and sensing gains, and the cavity pole frequencies. Thus the overall reconstructed strain is different from the initial astrophysical strain and noise received by the detector. The overall calibration uncertainty is quantified by

$$\frac{R(f;\lambda_{true})}{R(f;\lambda)} \tag{10}$$

where R is the detector response to gravitational waves, which is a function of frequency, f, and additional parameters, λ. The ratio between the measured response function, at the true value for λ and the modeled response function, at the theoretical parameter values,quantifies the amount that the reconstructed strain differs from the astrophysical strain and noise, displayed in figure 8. The white solid line in the center marks the systematic offset between measured and modeled response functions overall all frequencies, while the dashed lines correspond to the $\pm 1\sigma$ systematic calibration uncertainties in magnitude (above) and phase (below). Thus knowing how calibration uncertainty behaves as a function of frequency, for a given detector,

and due to the way frequency scales with redshift, we can determine the approximate calibration uncertainty levels at the frequency of the deformation signatures as a function of source redshift.

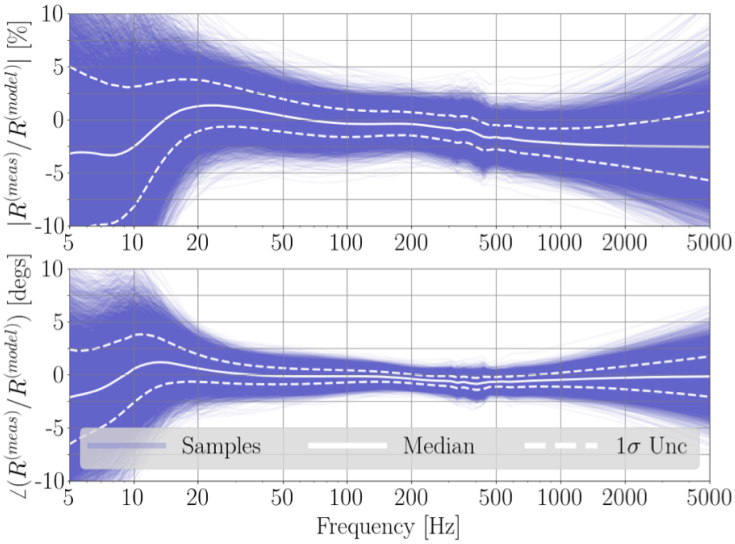

Figure 8: Calibration uncertainty budget for L1 [14]

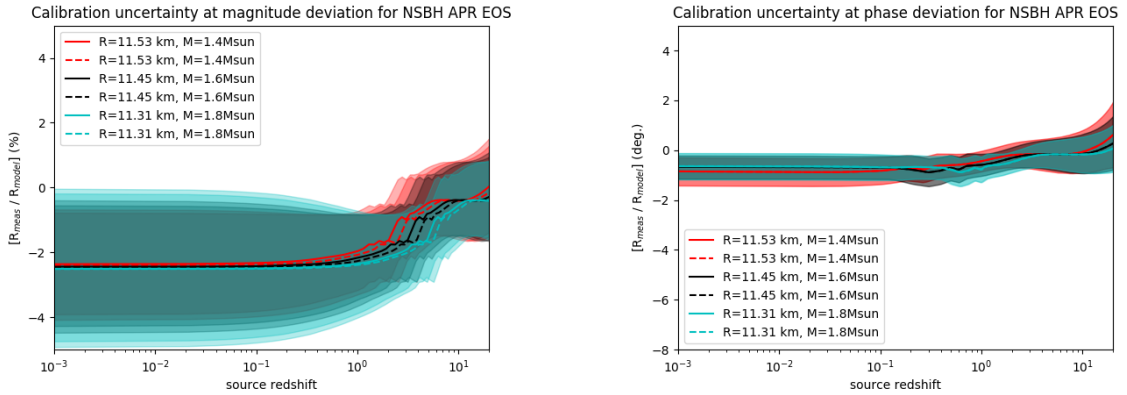

(a) Magnitude of calibration uncertainty

(b) Phase of calibration uncertainty

Figure 9: Calibration uncertainty at deformation signatures as a function of redshift for APR EOS

We plot the calibration uncertainty at the magnitude and phase deviation for both the APR and 2H EOS models. Once again we observe that the equation-of-state of the neutron star is a significant systematic bias, as the deformation signature is predicted to occur at a different frequency in magnitude and phase depending on the strength of the tidal parameter. In magnitude, we note that NSBH systems with a mass ratio of three have higher statistical calibration uncertainty levels for nearby sources, and a slightly greater overall systematic offset as compared with higher mass ratio systems. Systems with identical mass and tidal parameters, with a black hole of spin 0.5 have a greater systematic offset as compared to systems with non-spinning black holes. The most notable trend, however, is that for all the systems we examined, for both APR and 2H equation-of-state models, the magnitude calibration uncertainty at the deformation signature is worse for sources at low redshifts and improves significantly for higher redshift sources. One can motivate this by examining the overall calibration uncertainty budget for both L1 and H1; clearly, both systematic and statistical calibration uncertainty are at higher levels below 10 Hz and above 1 kHz; thus if we anticipate tidal signatures to be present in magnitude above 1kHz, there will be large calibration uncertainties in the gravitational waveform at the deformation signature until it is redshifted to a lower frequency, where the overall calibration uncertainty generally remains below three percent. Figure 6 suggests that a decline in the magnitude calibration uncertainty occurs around z $\approx$ 1. Einstein Telescope, with the ability to probe out to

redshifts of two with the threshold S/N, appears to have the capability of detecting deformation signatures for systems between redshifts of one and two with relatively high overall signal-to-noise ratios and low levels of calibration uncertainty. However, as we anticipate most NSBH sources to be closer than z $\approx$ 1, targeting lower calibration uncertainty in magnitude above 1 kHz will increase our chances of detecting matter signatures in NSBH waveform models, enabling us to do cosmography using information from gravitational wave signals alone.

If we examine the phase calibration uncertainty in an identical manner, we see that while a consistent systematic offset of about 1 degree exists for all redshifts, assuming the APR equation of state, the statistical errors are quite small in comparison to the statistical calibration uncertainty in magnitude. For the 2H equation of state, phase calibration uncertainty generally has the same width of statistical uncertainty, while the systematic offset is only a few tenths of a degree until a redshift of about 2 (which will be the limit of our reach with Einstein Telescope). Once again, in the high redshift regime, we do see a slight improvement in phase calibration uncertainty for the APR equation of state model; calibration uncertainty balloons out at high redshifts for the 2H equation of state as a result of the deformation frequency being redshifted down to tens of Hz.

Finally, in figure 7, we visualize the plus and minus one sigma statistical calibration uncertainty heatmaps for the APR equation of state model in magnitude and phase. This plot, in redshift-frequency space, indicates the color of the heatmap as the calibration uncertainty level at a given redshift and frequency. Because we anticipate most NSBH sources to be closer than z $\approx$ 1, targeting lower calibration uncertainty in magnitude above frequencies of 1 kHz will increase our chances of detecting matter signatures in NSBH waveform models. In phase, the statistical calibration uncertainty appears to have reached the fundamental limit of one degree, so improving the systematic offset will be most meaningful. Improvements in calibration uncertainty will enable us to do precision cosmography using information from gravitational wave signals alone.

4 Discussion and Conclusions

Aside from the limited analysis we discuss in this report, there exist several other systematic biases associated with our cosmography measurement. Below, we identify and briefly describe the main systematic biases that will affect our ability to do cosmography using the tidal deformation method.

• GW Malmquist Effect: This systematic bias arises from the inability to distinguish between sources that are face-on and sources that are nearby. Since our estimate of H_0 relies on both our ability to measure source redshifts and distances, this bias will contribute non-trivially to our final determination of H_0. A coincident electromagnetic counterpart, depending on its nature, could aid in breaking this distance-inclination angle degeneracy for tidally deforming BNS and NSBH systems.

• Equation of State: While at present we have only examined the 2H and APR EOS models in our analysis, there exist several other equations of state whose tidal λ parameters could yield vastly different frequencies of deformation in magnitude and phase. Thereby the methods we describe for analyzing whether cosmography will be possible with future detectors is more valuable than the actual values we obtain for the deformation signature frequencies. In addition, our research relies on the assumption that the neutron star is made of cold, degenerate matter, catayzed in the lowest energy state. We anticipate that by the 3G detector era, the equation of state of neutron stars will be known, and so will no longer majorly contribute to our systematic biases.

• Template waveform uncertainty: Our ability to observe deformation signatures depends on the accuracy of our template models of systems of different masses and spins. Though we use the latest waveform models, we are clearly limited in our parameter ranges, due to the fact that comprehensive waveform models are still being constructed. Waveform uncertainty will also be greatly reduced once we know the equation of state of neutron stars.

• Statistical Phase and Amplitude uncertainties: While our discussion includes contributions from calibration uncertainty, we do not address statistical uncertainties in phase and amplitude. Since statistical

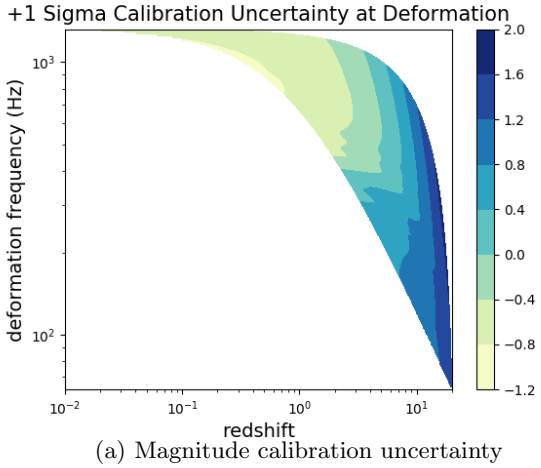

(a) Magnitude calibration uncertainty

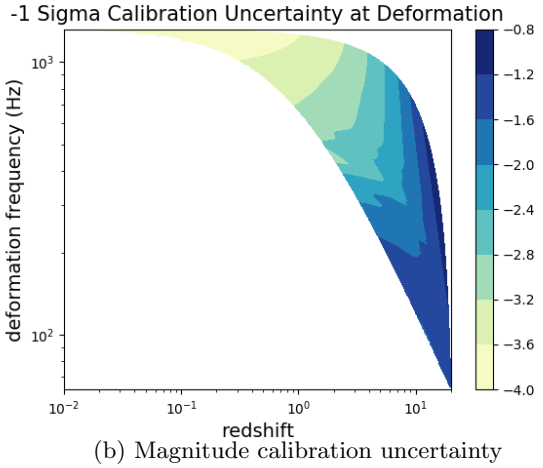

(b) Magnitude calibration uncertainty

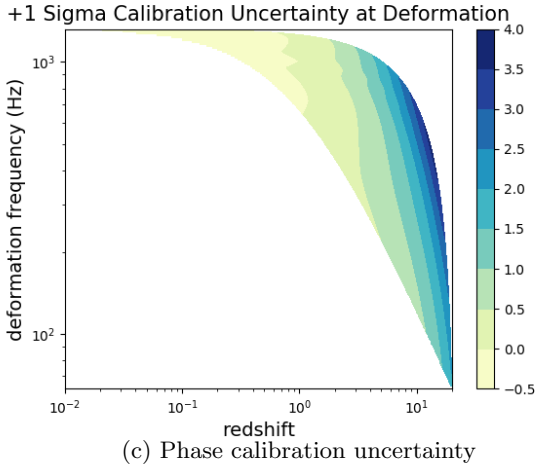

(c) Phase calibration uncertainty

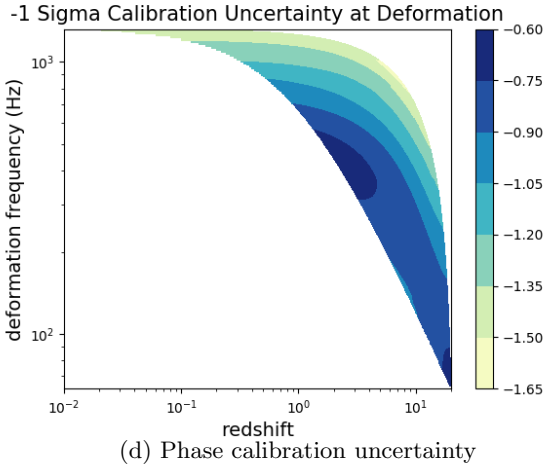

(d) Phase calibration uncertainty

Figure 10: Calibration uncertainty as a function of redshifted frequency and redshift at the deformation signature for APR EOS

phase uncertainty is inversely proportional to signal-to-noise ratio, we assume that for next generation detectors, for which we anticipate to have detections of far higher S/N on average, the statistical uncertainties will contribute less than calibration uncertainty. However, as we probe higher redshift systems, this assumption no longer holds true because the S/N will be much lower. In the future, we hope to extend this work by doing a Fisher matrix analysis of the amplitude, phase, and distance uncertainties to determine the precision with which we can determine H_0.

This work is the beginning of a larger undertaking to construct a viable method of constraining the Hubble constant and other cosmological parameters using gravitational wave observations alone. In our project, we analyze one possible method of determinining redshift to gravitational wave sources independently of the source distances using tidal signatures of matter. To do this, we simulate NSBH waveforms of different mass ratios and spins, for the 2H and APR equation of state models and identify the frequencies at which waveforms with matter differ from those without matter. Then, we recolor the datastream of Advanced LIGO with the noisecurve of Einstein Telescope and inject our simulated signal into the simulated datastream to try to recover the matter signatures. We find that identifying these signatures will be far easier in phase. However, for more distance systems, the deformation signatures will be redshifted down in band, allowing detection of deformation signatures even in magnitude. Finally, we outline calibration uncertainty requirements to resolve tidal signatures of matter for the purpose of cosmography.

Performing cosmography with gravitational waves successfully relies on the intersection between various disciplines in GW astrophysics; as we continue to constrain neutron star EOS, improve calibration uncer-

tainty, reduce noise levels, construct more accurate waveform models, and build future detector networks, we will have the unique chance to participate in gaining insight into the content and expansion history of the universe by constraining cosmological parameters.

5 References

1. Abbott, B.P. et al. (LIGO Scientific Collaboration) 2017, Phys. Rev. Lett. 118, 221101
2. Ngeow, C. and Kanbur, S. 2006, MNRAS, 396, 705
3. Sullivan, M. et al., 2011, ApJ 737, 102
4. P. A. R. Ade et al. (Planck Collaboration) 2015, A and A 594 A13
5. Sathyaprakash B.S., Schutz B.F. and C. V. Den Broeck 2009, Class. Quant. Grav. 27, 216006
6. Singer, L.P. et al. 2014, ApJ 795 105
7. Vitale, S. and Evans, M. 2016, Phys. Rev. D 95 064052
8. Abernathy, M. et al. (ET science team) 2011, ET-0106C-10, 4, 8-10
9. Zucker, M. et al. 2016, LIGO Document G1601435-v3
10. Abbott, B.P. et al. (LIGO Scientific Collaboration) 2016, arXiv:1607.08697
11. Messenger, C. et al. 2013, Phys. Rev. X 4 041004
12. Foucart, F. 2012, Phys. Rev. D 86 124007
13. Lackey, B. et al. 2017, Phys. Rev. D 95, 104036
14. E. Hall, C. Cahillane, K. Izumi, R. Smith, and R. Adhikari, LIGO Document 2017, P1700033-v3 [Draft]

6 Acknowledgements

I would like to thank my advisor, Alex Urban, for being a fantastic teacher, research advisor, and mentor during the SURF program, providing encouragement, help, and support all along the way. To Alan, Craig, TJ, and the remaining LIGO Lab faculty, thank you for providing your expertise on signal processing and calibration uncertainty, without which this work would not have been possible. Thank you, Leo, for providing me with a solid background on gravitational wave astrophysics to partake in this program, and for motivating me to present at Amaldi. Special thanks to Jocelyn and the Fullerton GWPAC group for their insights and collaboration on observing tidal deformation signatures. Finally I would like to acknowledge NSF and the LIGO Scientific Collaboration for creating and funding the Caltech SURF program.